Optimization of Perturb and Observe Maximum Power Point Tracking Method

Nicola Femia, *Member, IEEE*, Giovanni Petrone, Giovanni Spagnuolo, *Member, IEEE*, and Massimo Vitelli

***Abstract*—Maximum power point tracking (MPPT) techniques are used in photovoltaic (PV) systems to maximize the PV array output power by tracking continuously the maximum power point (MPP) which depends on panels temperature and on irradiance conditions. The issue of MPPT has been addressed in different ways in the literature but, especially for low-cost implementations, the perturb and observe (P&O) maximum power point tracking algorithm is the most commonly used method due to its ease of implementation. A drawback of P&O is that, at steady state, the operating point oscillates around the MPP giving rise to the waste of some amount of available energy; moreover, it is well known that the P&O algorithm can be confused during those time intervals characterized by rapidly changing atmospheric conditions. In this paper it is shown that, in order to limit the negative effects associated to the above drawbacks, the P&O MPPT parameters must be customized to the dynamic behavior of the specific converter adopted. A theoretical analysis allowing the optimal choice of such parameters is also carried out.**

Results of experimental measurements are in agreement with the predictions of theoretical analysis.

***Index Terms*—Maximum power point (MPP), maximum power point tracking (MPPT), perturb and observe (P&O), photovoltaic (PV).**

I. Introduction

A PHOTOVOLTAIC (PV) array under uniform irradiance exhibits a current-voltage characteristic with a unique point, called the maximum power point (MPP), where the array produces maximum output power [1].

In Fig. 1, an example of PV module characteristics in terms of output power versus voltage and current versus voltage for three irradiance levels S and two temperature values T are shown. The MPP point has been also evidenced in both figures.

As evidenced in Fig. 1, since the *I–V* characteristic of a PV array, and hence its MPP, changes as a consequence of the variation of the irradiance level and of the panels' temperature (which is in turn function of the irradiance level, of the ambient temperature, of the efficiency of the heat exchange mechanism and of the operating point of the panels) [1], it is necessary to track continuously the MPP in order to maximize the power output from a PV system, for a given set of operating conditions.

The issue of maximum power point tracking (MPPT) has been addressed in different ways in the literature: examples of fuzzy logic, neural networks, pilot cells and DSP based implementations have been proposed in [2]–[10]. Nevertheless, the perturb and observe (P&O) and INcremental Conductance (INC) [2] techniques are widely used, especially for low-cost implementations.

The P&O MPPT algorithm is mostly used, due to its ease of implementation. It is based on the following criterion: if the operating voltage of the PV array is perturbed in a given direction and if the power drawn from the PV array increases, this means that the operating point has moved toward the MPP and, therefore, the operating voltage must be further perturbed in the same direction. Otherwise, if the power drawn from the PV array decreases, the operating point has moved away from the MPP and, therefore, the direction of the operating voltage perturbation must be reversed.

A drawback of P&O MPPT technique is that, at steady state, the operating point oscillates around the MPP giving rise to the waste of some amount of available energy. Several improvements of the P&O algorithm have been proposed in order to reduce the number of oscillations around the MPP in steady state, but they slow down the speed of response of the algorithm to changing atmospheric conditions and lower the algorithm efficiency during cloudy days [11].

The INC algorithm seeks to overcome such limitations: it is based on the observation that, at the MPP it is $(di_{PV}/dv_{PV}) + (i_{PV}/v_{PV}) = 0$, where i_{PV} and v_{PV} are the PV array current and voltage, respectively. When the operating point in the V-P plane is on the right of the MPP, then $(di_{PV}/dv_{PV}) + (i_{PV}/v_{PV}) < 0$, whereas, when the operating point is on the left of the MPP, then $(di_{PV}/dv_{PV})+(i_{PV}/v_{PV}) > 0$. The sign of the quantity $(di_{PV}/dv_{PV}) + (i_{PV}/v_{PV})$ indicates the correct direction of perturbation leading to the MPP. By means of the INC algorithm it is therefore theoretically possible to know when the MPP has been reached and therefore when the perturbation can be stopped, whereas in the P&O implementation the operating point oscillates around the MPP. Indeed, as discussed in [12], because of noise and measurement and quantization errors, the condition $(di_{PV}/dv_{PV}) + (i_{PV}/v_{PV}) = 0$ is in practice never exactly satisfied, but it is usually required that such condition is approximately satisfied within a given accuracy. As a consequence, the INC operating voltage cannot be exactly coincident with the MPP and oscillates across it. A disadvantage of the INC algorithm, with respect to P&O, is in the increased hardware and software complexity; moreover, this latter leads to increased computation times and to the consequent slowing down of the possible sampling rate of array voltage and current.

Both P&O and INC methods can be confused during those time intervals characterized by changing atmospheric conditions, because, during such time intervals, the operating point can move away from the MPP instead of keeping close to it [2]. This drawback is shown in Fig. 2, where the P&O MPPT operating point path for an irradiance variation from 200 W/m^2 to

Manuscript received January 16, 2004; revised October 14, 2004. Recommended by Associate Editor Z. Chen.

N. Femia, G. Petrone, and G. Spagnuolo are with the Università di Salerno, Fisciano (SA), Italy (e-mail: femia@unisa.it; gpetrone@unisa.it; spanish@ieee.org).

M. Vitelli is with the Seconda Università di Napoli, Aversa (CE), Italy (e-mail: vitelli@unina.it).

Digital Object Identifier 10.1109/TPEL.2005.850975

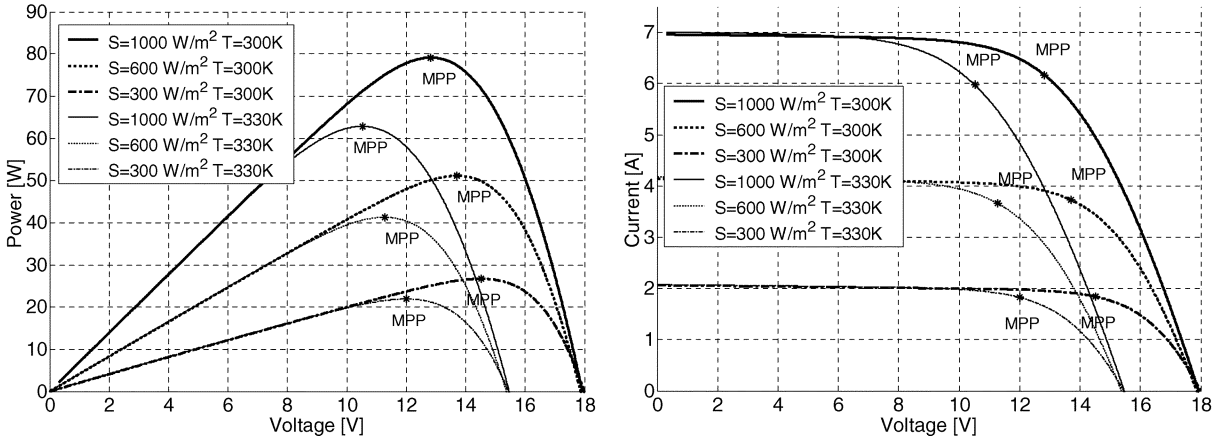

Fig. 1. PV module characteristics for three irradiance levels S and two different panels' temperature: (a) output power versus voltage and (b) current versus voltage.

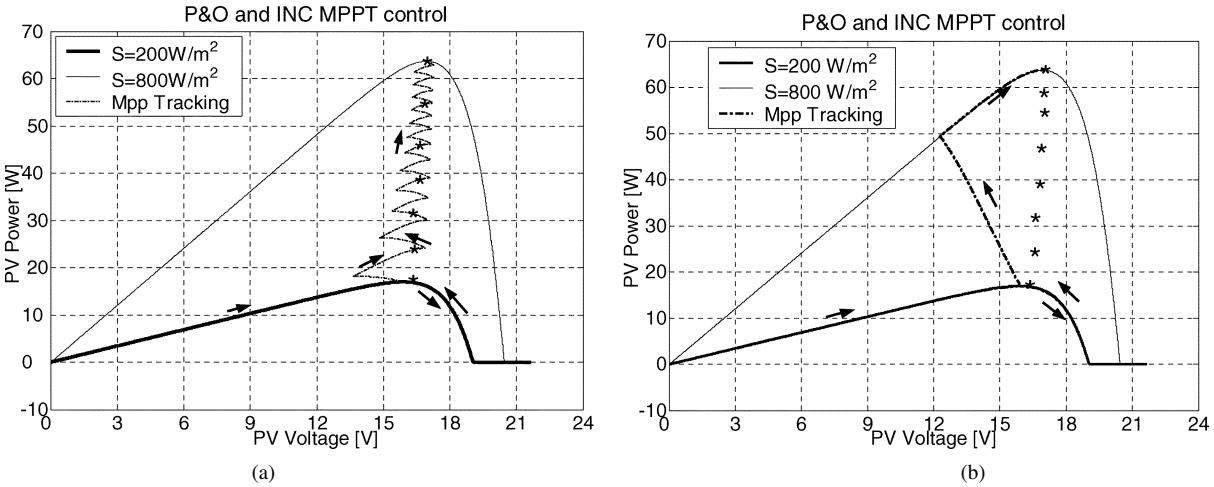

Fig. 2. P&O MPPT operating point path. The $*$ represents MPP for different levels of the irradiance: (a) slow change in atmospheric conditions and (b) rapid change in atmospheric conditions.

800 W/m^2 is reported. The example reports two different behaviors in the plane output power versus voltage. Fig. 2(a) shows the operating point path in presence of slowly changing atmospheric conditions and Fig. 2(b), instead, shows the failure of MPPT control to follow the MPP when a rapid change in atmospheric conditions occurs. Also the INC MPPT control presents such behavior.

There is no general agreement in the literature on which one of the two methods is the best one, even if it is often said that the efficiency—expressed as the ratio between the actual array output energy and the maximum energy the array could produce under the same temperature and irradiance level—of the INC algorithm is higher than that one of the P&O algorithm. To this regard, it is worth saying that the comparisons presented in the literature are carried out without a proper optimization of P&O parameters. In [12] it is shown that the P&O method, when properly optimized, leads to an efficiency which is equal to that obtainable by the INC method. These are often merely chosen on the basis of trial and error tests. Unfortunately, no guidelines or general rules are provided to determine the optimal values of P&O parameters. The present paper is devoted to fill such a hole [13].

A theoretical analysis allowing the optimal choice of the two main parameters characterizing the P&O algorithm is carried out. The key idea underlying the proposed optimization approach lies in the customization of the P&O MPPT parameters to the dynamic behavior of the whole system composed by the specific converter and PV array adopted. Results obtained by means of such approach clearly show that, in the design of efficient MPPT regulators, the easiness and flexibility of P&O MPPT control technique can be exploited by optimizing it according to the specific system's dynamic.

As an example, the boost converter reported in Fig. 3(a) is examined. Results obtained and the considerations that are drawn can be extended to any other converter topology as well.

The system in Fig. 3(a) can be schematically represented as in Fig. 3(b), where d is the duty cycle and p is the power drawn from the PV array. In the following, the sampling interval will be indicated with T_a, and the amplitude of the duty cycle perturbation with $\Delta \mathrm{d} = |\mathrm{d}(\mathrm{kT_A}) - \mathrm{d}((k-1)T_a)| > 0$.

In the P&O algorithm the sign of the duty cycle perturbation at the $(k+1)$-th sampling is decided on the basis of the sign of the difference between the power $P((k+1)T_a)$ and the power $P(\mathrm{kT_A})$ according to the rules discussed above

$$\mathrm{d}\left((k+1)T_a\right) = \mathrm{d}(\mathrm{kT_A}) + \left(\mathrm{d}(\mathrm{kT_A}) - \mathrm{d}\left((k-1)T_a\right)\right) \cdot \mathrm{sign}\left(P\left((k+1)T_a\right) - P(\mathrm{kT_A})\right). \quad (1)$$

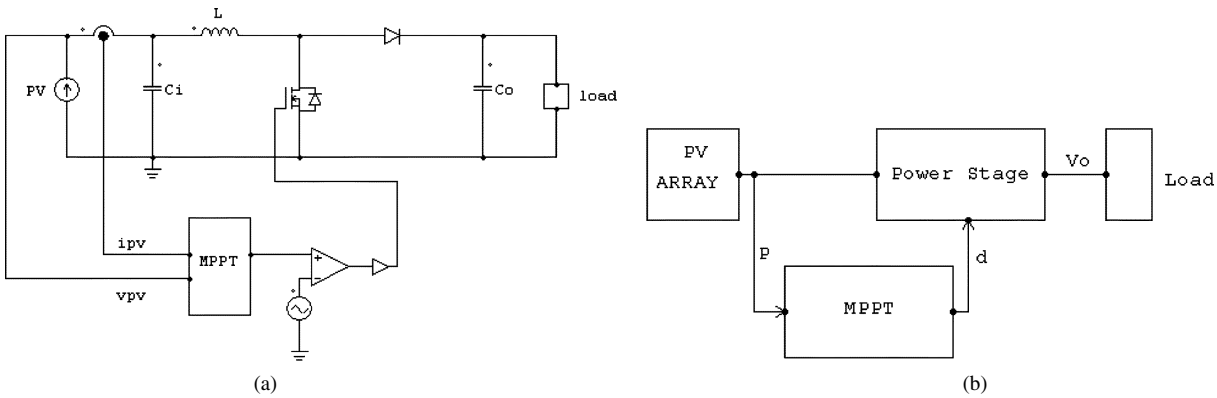

(a) (b)

Fig. 3. Boost converter with MPPT control: (a) simplified circuit and (b) equivalent block diagram.

The amplitude of the duty cycle perturbation is one of the two parameters requiring optimization: lowering Δd reduces the steady-state losses caused by the oscillation of the array operating point around the MPP; however, it makes the algorithm less efficient in case of rapidly changing atmospheric conditions. The optimal choice of Δd in these situations, when we have to account for both the source's and converter's dynamics, is discussed in detail in Section III. Besides the case of quickly varying MPP, which occurs in cloudy days only, there is a more general problem, connected to the choice of the sampling interval T_a used by the P&O MPPT algorithm, which arises even during sunny days, when the MPP moves very slowly. The sampling interval T_a should be set higher than a proper threshold in order to avoid instability of the MPPT algorithm and to reduce the number of oscillations around the MPP in steady state. In fact, considering a fixed PV array MPP, if the algorithm samples the array voltage and current too quickly, it is subjected to possible mistakes caused by the transient behavior of the whole system (PV array+converter), thus missing, even if temporarily, the current MPP of the PV array, which is in steady-state operation. As a consequence, the energy efficiency decays as the algorithm can be confused and the operating point can become unstable, entering disordered and/or chaotic behaviors [12]. To avoid this, it must be ensured that, after each duty-cycle perturbation, the system reaches the steady-state before the next measurement of array voltage and current is done. In Section II the problem of choosing T_a is analyzed and an optimized solution, based on the tuning the P&O algorithm according to converter's dynamics, is proposed. In Section III the optimization procedure is illustrated for rapidly varying irradiance conditions. Section IV introduces experimental verifications and Section V is devoted to conclusions.

II. Steady-State Operation

Let us suppose that the system is working at steady-state, under constant and uniform irradiance level, and that the MPP has been reached. If the operating point of the PV array lies in a sufficiently narrow interval around the MPP, the power drawn by the PV array can be expressed as

$$P(t) \cong \frac{\mathrm{v}_{PV}^2(t)}{R_{\mathrm{MPP}}} \tag{2}$$

where $R_{\mathrm{MPP}} = \mathrm{V}_{\mathrm{MPP}}/I_{\mathrm{MPP}}$, with $\mathrm{V}_{\mathrm{MPP}}$ and I_{MPP} the PV array MPP voltage and current, respectively.

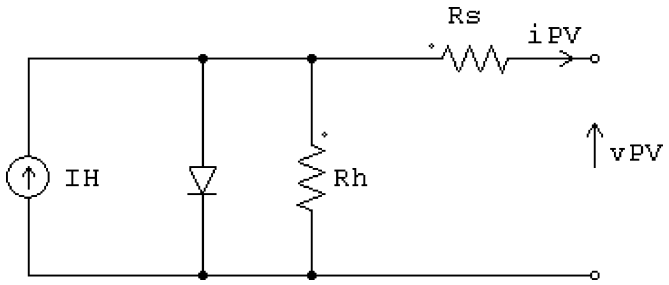

Fig. 4. Equivalent circuit of a PV array.

The PV array power is maximum when the adapted load resistance R equals the absolute value R_{MPP} of the differential resistance of the PV array at the MPP. In order to identify the minimum value to assign to T_a, the behavior of the system forced by a small duty-cycle step perturbation must be analyzed. In fact, in order to allow the MPPT algorithm to make a correct interpretation of the effect of a duty-cycle step perturbation on the corresponding steady-state variation of the array output power p, it is necessary that the time between two consecutive samplings is long enough to allow p to reach its steady state value.

The equivalent circuit of a PV array is shown in Fig. 4.

The relation between the array terminal current and voltage is the following [1]:

$$i_{\mathrm{PV}} = I_{\mathrm{H}} - I_{\mathrm{S}} \cdot \left(\mathrm{e}^{\frac{\mathrm{v}_{PV} + R_s \cdot i_{\mathrm{PV}}}{\eta \cdot \mathrm{V}_T}} - 1 \right) - \frac{\mathrm{v}_{PV} + R_s \cdot i_{\mathrm{PV}}}{R_{\mathrm{h}}} \tag{3}$$

where R_{S} and R_{h} are series and shunt resistances, respectively, I_{H} is the light induced current, η is the diode ideality factor, I_{S} is the diode saturation current and V_T is the thermal voltage. I_{H} depends on the irradiance level S and on the array temperature T, while I_{S} and V_T depend on T only [1]. The PV array current i_{PV} is a nonlinear function of the PV array voltage v_{PV}, of the irradiance level S and of the temperature T. If the oscillations of the operating point $(\mathrm{v}_{PV}, i_{\mathrm{PV}})$ are small compared to $(\mathrm{V}_{\mathrm{MPP}}, I_{\mathrm{MPP}})$, then the relationship among i_{PV}, v_{PV}, S and T can be linearized as

$$\hat{i}_{\mathrm{PV}} = \left.\frac{\partial i_{\mathrm{PV}}}{\partial \mathrm{v}_{PV}}\right|_{\mathrm{MPP}} \cdot \hat{\mathrm{v}}_{PV} + \left.\frac{\partial i_{\mathrm{PV}}}{\partial \mathrm{s}}\right|_{\mathrm{MPP}} \cdot \hat{\mathrm{s}} + \left.\frac{\partial i_{\mathrm{PV}}}{\partial T}\right|_{\mathrm{MPP}} \cdot \hat{T} \tag{4}$$

where symbols with hats represent small-signal variations around the steady state values of the corresponding quantities. At constant irradiance level, it is $\hat{\mathrm{s}} = 0$. Moreover, at steady-state, due to the relatively high thermal inertia of the PV array

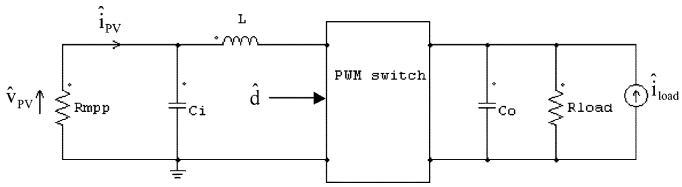

Fig. 5. Small signal equivalent circuit.

[1], the variations of the PV array temperature, as a consequence of small oscillations of the operating point, are certainly negligible: then $\hat{T} \approx 0$. Therefore, (4) can be rewritten as

$$\hat{i}_{\rm PV} = \left.\frac{\partial i_{\rm PV}}{\partial {\rm v}_{PV}}\right|_{\rm MPP} \cdot \hat{\rm v}_{PV}. \tag{5}$$

From (3) we get

$$\left.\frac{\partial i_{\rm PV}}{\partial {\rm v}_{PV}}\right|_{\rm MPP} = -\left[R_{\rm S} + \frac{1}{\frac{I_{\rm S}}{\eta \cdot {\rm V}_T} \cdot {\rm e}^{\frac{{\rm V}_{\rm MPP}+R_{\rm S}\cdot I_{\rm MPP}}{\eta \cdot {\rm V}_T}} + \frac{1}{R_{\rm h}}}\right]^{-1} = -\frac{1}{R_{\rm MPP}}. \tag{6}$$

In the neighborhood of the MPP we have

$$\begin{aligned} {\rm v}_{PV} &= {\rm V}_{\rm MPP} + \hat{\rm v}_{PV} \\ i_{\rm PV} &= I_{\rm MPP} + \hat{i}_{\rm PV} \\ P &= P_{\rm MPP} + \hat{P} = {\rm V}_{\rm MPP} I_{\rm MPP} + {\rm V}_{\rm MPP}\hat{i}_{\rm PV} \\ &\quad + \hat{\rm v}_{PV} I_{\rm MPP} + \hat{\rm v}_{PV}\hat{i}_{\rm PV}. \end{aligned} \tag{7}$$

From (5)–(7), by using the condition that at MPP ${\rm V}_{\rm MPP} = R_{\rm MPP} I_{\rm MPP}$, we get

$$\begin{aligned} P_{\rm MPP} &= {\rm V}_{\rm MPP} I_{\rm MPP} \\ \hat{P} &= {\rm V}_{\rm MPP}\hat{i}_{\rm PV} + \hat{\rm v}_{PV} I_{\rm MPP} + \hat{\rm v}_{PV}\hat{i}_{\rm PV} \\ &= \hat{\rm v}_{PV}\left(I_{\rm MPP} - \frac{{\rm V}_{\rm MPP}}{R_{\rm MPP}}\right) + \hat{\rm v}_{PV}\hat{i}_{\rm PV} \\ &= -\frac{\hat{\rm v}_{PV}^2}{R_{\rm MPP}}. \end{aligned} \tag{8}$$

This is a general result which is not dependent on the adopted converter topology. On the basis of (8), in order to investigate the performances of an MPPT algorithm it is useful to study the control-to-array voltage transfer function, as explained in the following.

The small signal equivalent circuit of the system under study is represented in Fig. 5.

As for the technique of circuit averaging from which PWM switch models can be derived, the interested reader can find a comprehensive treatment in [14] and in references cited therein.

The circuit of Fig. 5, assumed to operate in continuous conduction mode, can be analyzed to find the small signal control to

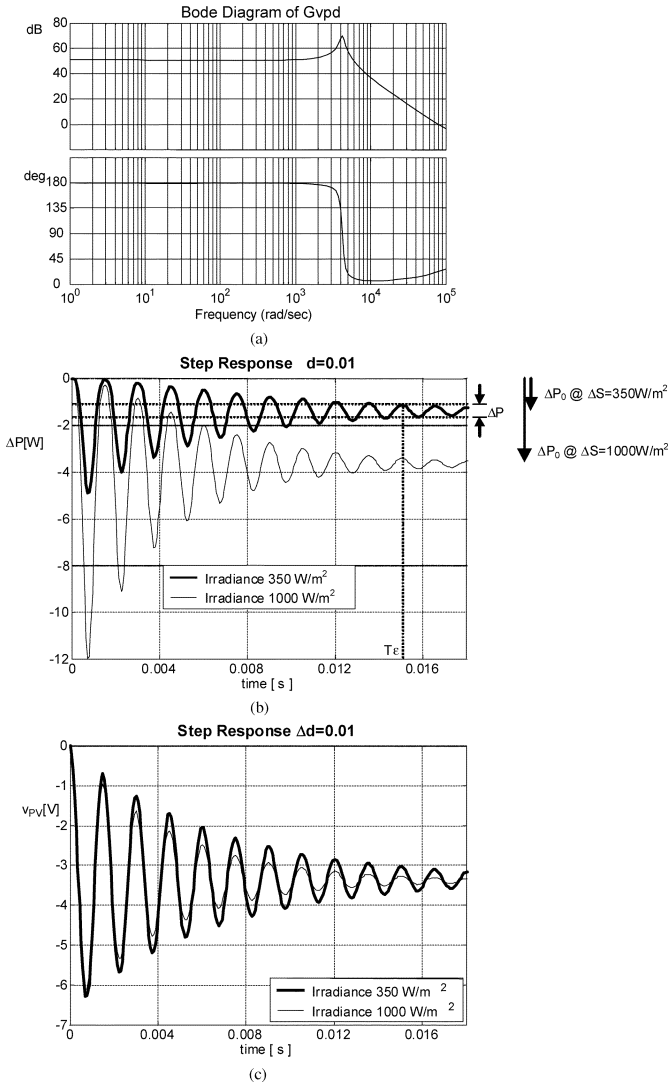

Fig. 6. (a) Bode diagrams and (b) step response of $\hat{P}$ and (c) step responses of $\hat{\rm v}_{PV}$.

array voltage transfer function $G_{v_p^d}$ and the load to array voltage transfer function $G_{v_p^{\rm load}}$

$$\hat{\rm v}_{PV} = G_{v_p^{\rm load}} \cdot \hat{\rm d} + G_{{\rm V}_P{\rm load}} \cdot \hat{i}_{\rm load}. \tag{9}$$

In the case of an ideal converter model, obtained by neglecting parasitic resistances, the transfer functions $G_{v_p^{\rm load}}$ and $G_{v_p^{\rm load}}$ of the power stage assume (10a) and (10b), shown at the bottom of the page, where D is the steady state duty cycle and $\rm V_o$ is the output voltage.

The transfer function $G_{{\rm V}_P{\rm load}}$ is useful in order to study the variations of the array voltage caused by load changes; such variations can confuse the MPPT algorithm which is not able to

$$G_{v_p^d}({\rm s}) = -\frac{V_o}{L \cdot C_i \cdot s^2 + \left(\frac{L}{R_{\rm load}\cdot(1-D)^2}\right) \cdot s + 1} \tag{10a}$$

$$G_{{\rm V}_P{\rm load}}({\rm s}) = \frac{R_{\rm load} \cdot (1-D)}{LC_i R_{\rm load} C_o s^3 + \left(C_i + \frac{C_o}{(1-D)^2}\right) L \cdot s^2 + \left(R_{\rm load}\left(C_i(1-D)^2 + C_o\right) + \frac{L}{R_{\rm load}\cdot(1-D)^2}\right) \cdot s + 2} \tag{10b}$$

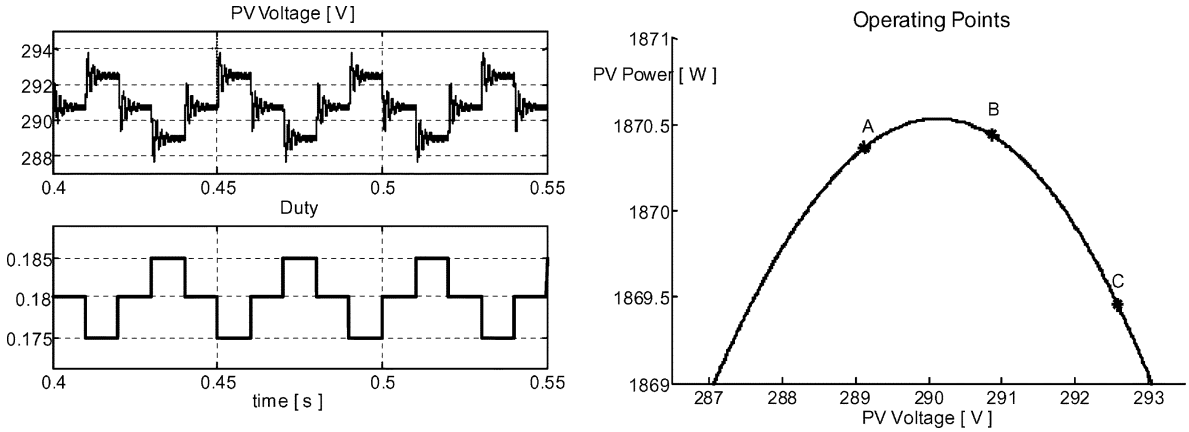

Fig. 7. Simulations with: ε =0.1, T_a = 0.01 s, Δd =0.005, S = 1000 W/m^2: (a) time domain waveforms and (b) operating points location on PV characteristic.

distinguish between array voltage oscillations caused by the load change or by the modulation of the duty. The transfer function $G_{\mathrm{V}_P\mathrm{load}}$ assumes different relevance depending on the application. In the case of a battery charger, for example, the battery plays as an ideal voltage source in place of the resistor R_{load}. In such conditions, the variation of the load current (represented by means of a current source placed in parallel with the battery) has no impact on the array voltage and therefore the load to array voltage transfer function is equal to zero: $G_{\mathrm{V}_P\mathrm{load}} = 0$. In grid-connected applications, instead, the transfer function $G_{\mathrm{V}_P\mathrm{load}}$ must be considered in order to analyze the propagation of 100/120 Hz perturbations from grid to PV array. In the following, for sake of simplicity, the first case is analyzed and the attention will be focused on $G_{v_p^d}$. Named R_{in} the equivalent resistance at the converter's input, by assuming the maximum power transfer, $R_{\mathrm{in}} = R_{\mathrm{MPP}}$, and remembering that, for a ideal boost converter [14], $R_{\mathrm{in}} = R_{\mathrm{load}} \cdot (1 - \mathrm{D})^2$, the transfer function $G_{v_p^d}$ assumes

$$G_{v_p^d}(\mathrm{s}) = \frac{\mu \cdot \omega_n^2}{s^2 + 2 \cdot \xi \cdot \omega_n \cdot s + \omega_n^2} \tag{11}$$

where $\mu = -\mathrm{V_o}$, $\omega_\mathrm{n} = 1/\sqrt{L \cdot C_i}$ and $\xi = 1/(2 \cdot R_{\mathrm{MPP}}) \cdot \sqrt{L/C_i}$.

Note that R_{load} has to be considered as the ratio between output voltage an current; so that (11), where the dependence of $G_{v_p^d}$ on R_{MPP} rather than on R_{load} has been evidenced, has general validity.

According to the transfer function (11), the response of $\hat{\mathrm{v}}_{PV}$ to a small duty-cycle step perturbation of amplitude Δd is

$$\hat{\mathrm{v}}_{PV} = \mu \Delta \mathrm{d} \left(1 - \frac{1}{\sqrt{1-\xi^2}} \cdot \mathrm{e}^{-\xi \cdot \omega_\mathrm{n} \cdot T} \cdot \sin\left(\omega_\mathrm{n} \cdot T \cdot \sqrt{1-\xi^2} + \arccos(\xi) \right) \right). \tag{12}$$

On the basis of (8) and (12), the response of $\hat{P}$ to a small duty cycle step perturbation of amplitude Δd can be approximated as shown in

$$\hat{P} = -\frac{\hat{\mathrm{v}}_{PV}^2}{R_{\mathrm{MPP}}} \approx -\frac{\mu^2 \Delta \mathrm{d}^2}{R_{\mathrm{MPP}}} \left(1 - \frac{2}{\sqrt{1-\xi^2}} \cdot \mathrm{e}^{-\xi \cdot \omega_\mathrm{n} \cdot T} \cdot \sin\left(\omega_\mathrm{n} \cdot T \cdot \sqrt{1-\xi^2} + \arccos(\xi) \right) \right). \tag{13}$$

Therefore, $\hat{P}$ will keep in the range $[\Delta P_0 - \Delta P_\varepsilon/2, \Delta P_0 + \Delta P_\varepsilon/2]$, where $\Delta P_0 = -\mu^2 \Delta \mathrm{d}^2 / R_{\mathrm{MPP}}$, after the time

$$T_\varepsilon \cong -\frac{1}{\xi \cdot \omega_\mathrm{n}} \cdot \ln(\varepsilon) \tag{14}$$

where $\varepsilon = \Delta P_\varepsilon / (2|\Delta P_\mathrm{o}|)$. In the analysis and characterization of dynamic systems, $\varepsilon = 0.1$ is commonly assumed as a reasonable threshold to consider the transient over. So that, in order that the MPPT in not affected by mistakes caused by intrinsic transient oscillations of the PV system, the choice $T_a \geq T_{0.1}$ can be done. For example, let us consider a PV array composed by fourteen panels connected in series with a total surface of about 14 m^2, for which $R_{\mathrm{MPP}} = 45\ \Omega$ (at s = 1000 W/m^2), $R_{\mathrm{MPP}} = 120\,\Omega$ (at s = 350 W/m^2), and let the values of the circuit parameters be the following: $L = 600\ \mu$H, $R_L = 300$ mΩ (equivalent inductor series resistance) $C_i = 100\ \mu$F, $R_{\mathrm{Ci}} = 50$ mΩ (equivalent capacitor series resistance), $\mathrm{V_o} = 350$ V, switching frequency $\mathrm{f_S} = 25$ kHz. If the parasitic resistances are taken into account, the ξ factor assumes the expression: $\xi = 1/(2 \cdot R_{\mathrm{MPP}}) \cdot \sqrt{L/C_i} + ((R_{Ci} + R_L)/2) \cdot \sqrt{C_i/L}$.

Consequently, ξ =0.091 (at s = 1000 W/m^2), ξ =0.087 (at s = 350 W/m^2), and $\omega_\mathrm{n} = 4082$ rad/s. The resistance R_{Ci} introduces also a high frequency zero in the $G_{v_p^d}$ transfer function but it does not affect the MPPT analysis. The corresponding Bode diagrams of $G_{v_p^d}$ are shown in Fig. 6(a). In Fig. 6(b) and (c) the responses of $\hat{P}$ and $\hat{\mathrm{v}}_{PV}$ to a small (Δd =0.01) duty cycle step perturbation are respectively shown.

In Fig. 7 a detailed view of the PV array voltage and of the duty cycle for the P&O controlled boost battery charger with ε =0.1, T_a = 0.01 s, Δd = 0.005 and S = 1000 W/m^2 is shown. By using (14) we have $T_{0.1} = 0.007$ s. It is evident that a sufficiently low value of ε ensures that, if $T_a \geq T_\varepsilon$, then the P&O MPPT algorithm is not confused by the transient behavior of the system and the duty cycle oscillates assuming only three different values: $\{\mathrm{d_{MPP}} - \Delta\mathrm{d}, \mathrm{d_{MPP}}, \mathrm{d_{MPP}} + \Delta\mathrm{d}\}$ [Fig. 7(a)]. Correspondingly, for the boost battery charger, the operating point assumes only the following three different positions on the PV array characteristic of Fig. 7(b):

1) position A, on the left of the MPP and characterized by a PV array voltage lower than $\mathrm{V_{MPP}}$;
2) position B nearly coincident with the MPP;
3) position C, on the right of the MPP and characterized by a PV array voltage higher than $\mathrm{V_{MPP}}$.

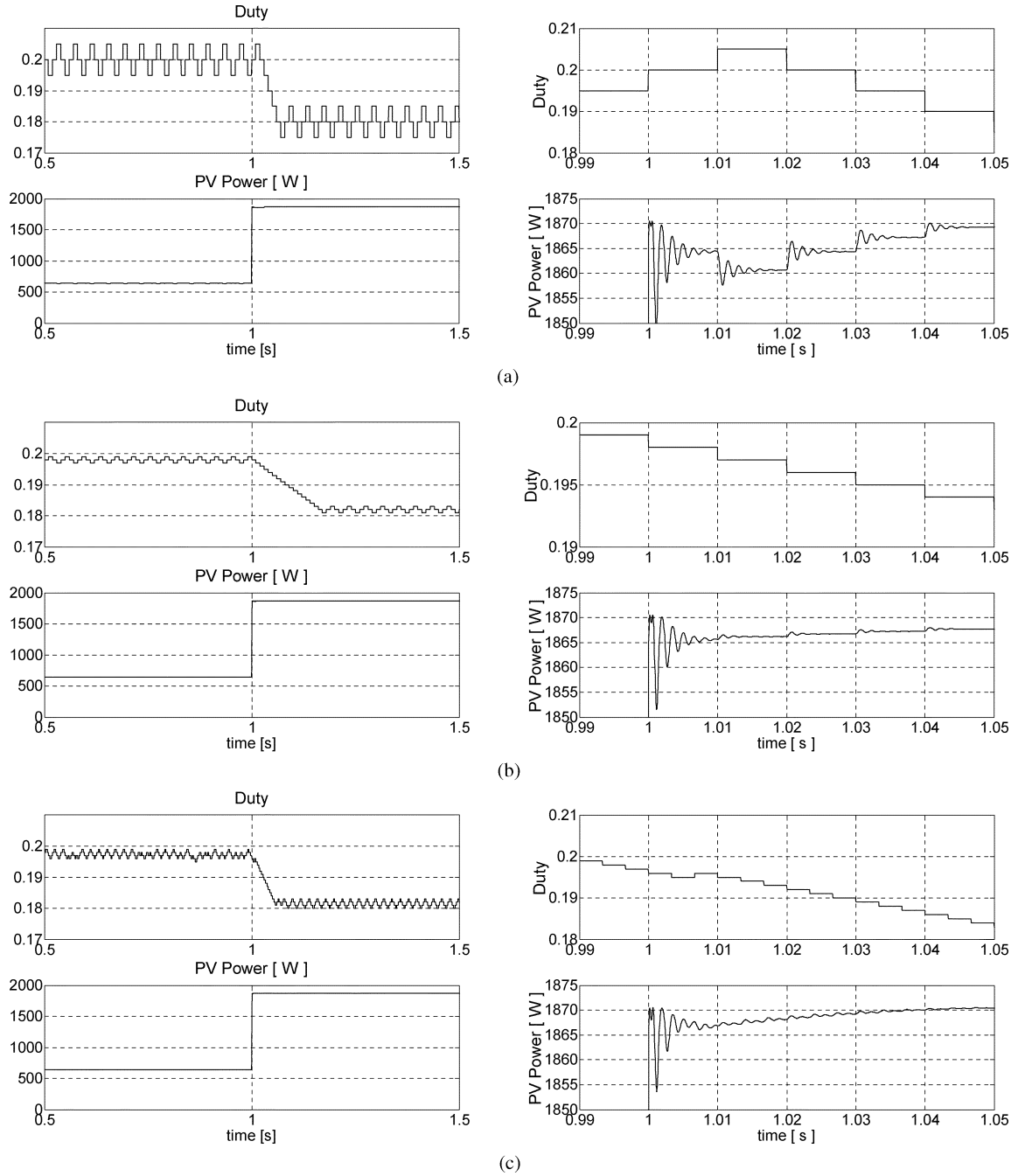

Fig. 8. Time domain simulations: (a) Δd $= 0.005$, $T_a = 0.01$ s; (b) Δd $= 0.001$, $T_a = 0.01$ s, (c) Δd $= 0.001$, $T_a = 0.0033$ s.

It is worth noting that the operating point B is not perfectly coincident with the MPP because of the discretization of the duty cycle; of course, the lower Δd the lower either the distance between B and the MPP or the speed of response of the algorithm to changing atmospheric conditions. Before each new perturbation of the duty-cycle, the oscillation of the PV array voltage, and hence of the PV array power, vanishes.

The choice of the value of T_a according to the proposed approach ensures a three-level steady-state duty-cycle swing around the MPP, whatever duty-cycle step-size Δd and irradiance level S are settled, as shown in the plots of the duty-cycle reported in Fig. 8, obtained with $T_a = 0.01$ s, Δd $=0.005$ [Fig. 8(a), Δd $=0.001$ [Fig. 8(b)] and with an irradiance step change from $S = 350$ W/m^2 to $S = 1000$ W/m^2.

As a consequence of the assumed step change of the irradiance level S, a correspondent change of the PV power takes place as evidenced in Fig. 8.

Fig. 8(c) shows, instead, that a lower value of T_a ($T_a = 0.0033$ s) leads to a worse behavior of the system, which is characterized, at both irradiance levels s $= 350$ W/m^2 and $S = 1000$ W/m^2, by a wider swing of the operating point around the MPP and then by a lower efficiency with respect to the corresponding case ($T_a = 0.01$ s) shown in Fig. 8(b). Moreover, in Fig. 8(c) at lower irradiance level, a non repetitive duty cycle behavior is also evident; this feature is in agreement with the experimental results reported in [1].

The plots of Fig. 8 also show the PV power transients from the steady-state value of 639 W, corresponding to 350 W/m^2

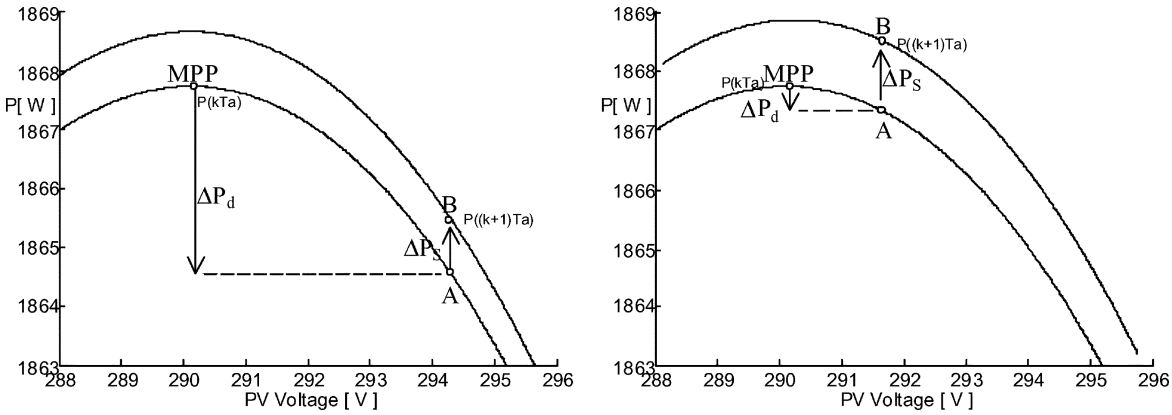

Fig. 9. Operating point of PV battery charger in presence of an irradiance variation. (a) Effect of a properly Δd choice. (b) Effect of a wrong Δd choice.

irradiation level for $t < 1$ s, to the steady-state value of 1871 W, corresponding to the irradiation level 1000 W/m^2 for $t > 1$ s.

The previous discussion puts in evidence that the optimal value of T_a does depend on the type of PV panels. This means that two possible strategies can be adopted to settle this MPPT control parameter: the easiest one consists in taking the maximum T_a value valid for all the possible arrangements of commercial panels of interest for given ranges of PV array voltage and current, while the optimal one consists in realizing a self-tuning system. This last is the subject of the authors' present research investigations.

III. Rapidly Changing Irradiance Conditions

As discussed in Section II, the sampling interval T_a should be set higher than a proper threshold in order to avoid instability of the MPPT algorithm and to reduce the number of oscillations across the MPP in steady state. The amplitude of the duty cycle perturbation Δd also requires some optimization: lowering Δd reduces the steady-state losses caused by the oscillation of the array operating point around the MPP but makes the algorithm less efficient in case of rapidly changing irradiance conditions. The optimal choice of Δd will be discussed in detail in this section.

A drawback of P&O is that it can be confused during those time intervals characterized by rapidly changing atmospheric conditions [2]. The possible failure of the P&O algorithm in presence of varying irradiance is due to the fact that the algorithm is not able to distinguish the variations of the output power caused by the duty cycle modulation from those ones caused by the irradiance variation. Let us suppose that the boost battery charger of the previous example is working at the MPP in the kth sampling instant (Fig. 9), at an irradiance level equal to S, and that the sign of the duty-cycle perturbation is negative $\mathrm{d}(k) = \mathrm{d}(k-1) - \Delta\mathrm{d}$: consequently, the operating point must move in the direction of higher array voltages from the MPP to point A. If the irradiance level changes between the k-th and the $(k+1)$-th sampling instants, for example if it increases (Fig. 9), then the operating point at the $(k+1)$-th sampling will be point B instead of point A. In the sequel ΔP_{d} is the array output power variation (at a constant irradiance level S) caused by the P&O driven duty cycle variation and ΔP_{S} is the array output power variation (at a constant duty cycle $\mathrm{d}(k) = \mathrm{d}((k-1)T_a) - \Delta\mathrm{d}$) caused by the variation Δs of the irradiance level. The algorithm will not be confused only if

$$|\Delta P_{\mathrm{d}}| > |\Delta P_{\mathrm{S}}|. \tag{15}$$

In the case shown in Fig. 9(a), the inequality (15) is satisfied and the algorithm is not confused, as it correctly provides $\mathrm{d}((k+1)T_a) = \mathrm{d}(kT_a) + \Delta\mathrm{d}$ so that the operating point moves back to the MPP; in the case shown in Fig. 9(b), instead, the algorithm is confused and provides $\mathrm{d}((k+1)T_a) = \mathrm{d}(kT_a) - \Delta\mathrm{d}$ so that the operating point further moves in the direction of increasing array voltages, away from the MPP.

In the following, current and voltage variations with respect to the MPP, at a constant irradiance level, will be indicated as ΔI_{d} and $\Delta \mathrm{V}_{\mathrm{d}}$ respectively. Accordingly, we get

$$\Delta P_{\mathrm{d}} = \mathrm{V}_{\mathrm{MPP}}\Delta I_{\mathrm{d}} + I_{\mathrm{MPP}}\Delta \mathrm{V}_{\mathrm{d}} + \Delta \mathrm{V}_{\mathrm{d}}\Delta I_{\mathrm{d}}. \tag{16}$$

If the oscillations of the operating point are small compared to the MPP then, on the basis of (3), ΔI_{d} can be approximated as

$$\Delta I_{\mathrm{d}} \approx \left.\frac{\partial i_{\mathrm{PV}}}{\partial \mathrm{v}_{PV}}\right|_{\mathrm{MPP}} \Delta \mathrm{V}_{\mathrm{d}} + \frac{1}{2}\left.\frac{\partial^2 i_{\mathrm{PV}}}{\partial^2 \mathrm{v}_{PV}}\right|_{\mathrm{MPP}} \Delta \mathrm{V}_{\mathrm{d}}^2 \tag{17}$$

where

$$\begin{aligned}\left.\frac{\partial i_{\mathrm{PV}}}{\partial \mathrm{v}_{PV}}\right|_{\mathrm{MPP}} &= -\frac{1}{R_{\mathrm{MPP}}}; \frac{1}{2}\left.\frac{\partial^2 i_{\mathrm{PV}}}{\partial^2 \mathrm{v}_{PV}}\right|_{\mathrm{MPP}} \\ &= -\frac{1}{2}\frac{1}{\eta \cdot \mathrm{V}_T} \cdot \left(\frac{1 - R_{\mathrm{S}}}{R_{\mathrm{MPP}}}\right)^3 \\ &\quad \cdot \left(\frac{I_{\mathrm{S}}}{\eta \cdot \mathrm{V}_T} \cdot \mathrm{e}^{\frac{\mathrm{V}_{\mathrm{MPP}} + R_{\mathrm{S}} \cdot I_{\mathrm{MPP}}}{\eta \cdot \mathrm{V}_T}}\right) = -\mathrm{H}. \end{aligned} \tag{18}$$

On the basis of (17) and (18), and considered that $\mathrm{V}_{\mathrm{MPP}} = R_{\mathrm{MPP}} I_{\mathrm{MPP}}$, (16) can be rewritten as

$$\begin{aligned}\Delta P_{\mathrm{d}} &\approx \left(I_{\mathrm{MPP}} - \frac{\mathrm{V}_{\mathrm{MPP}}}{R_{\mathrm{MPP}}}\right)\Delta \mathrm{V}_{\mathrm{d}} - \left(\mathrm{H}\mathrm{V}_{\mathrm{MPP}} + \frac{1}{R_{\mathrm{MPP}}}\right)\Delta \mathrm{V}_{\mathrm{d}}^2 \\ &= -\left(\mathrm{H}\mathrm{V}_{\mathrm{MPP}} + \frac{1}{R_{\mathrm{MPP}}}\right)\Delta \mathrm{V}_{\mathrm{d}}^2. \end{aligned} \tag{19}$$

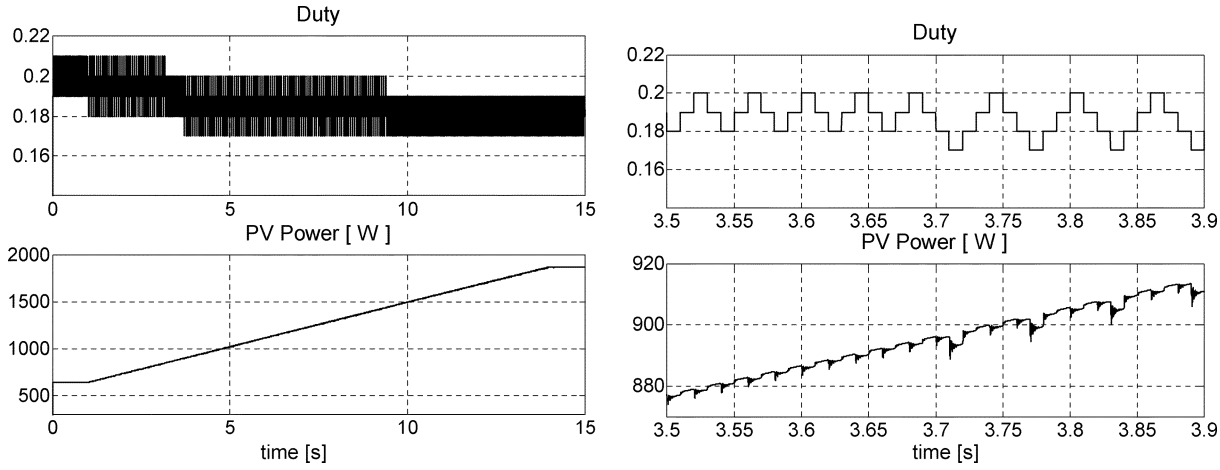

Fig. 10. Simulation results for: $T_a = 0.01$ s; Δd =0.01; $\dot{\mathrm{s}} = 50\ \mathrm{W/(m^2 s)}$; (b) zoom of (a).

If a first order approximation is used for ΔI_{d}, instead of (18), then we get $\Delta P_{\mathrm{d}} \approx 0$, if the quantity $\Delta \mathrm{V_d} \Delta I_{\mathrm{d}}$ is neglected in (16), or $\Delta P_{\mathrm{d}} \approx -(\Delta \mathrm{V_d^2}/R_{\mathrm{MPP}})$ if $\Delta \mathrm{V_d} \Delta I_{\mathrm{d}}$ is not neglected in (16). In any case, both expressions are coarse approximations that do not allow us to check, with adequate accuracy, whether inequality (15) is verified or not. The effect of a duty-cycle step perturbation of amplitude Δd on the corresponding steady-state variation $\Delta \mathrm{V_d}$ of the array voltage can be evaluated by using the small signal control to array voltage transfer function $G_{v_p^d}$ introduced in Section II

$$\Delta \mathrm{V_d} = G_{\mathrm{o}} \cdot \Delta \mathrm{d} \tag{20}$$

where G_0 is the dc gain of $G_{v_p^d}$. As for ΔP_{s}, by neglecting $\Delta \mathrm{V_d}$ with respect to $\mathrm{V_{MPP}}$, we get

$$\Delta P_{\mathrm{s}} = \mathrm{V_{MPP}} \Delta I_{\mathrm{s}} + \Delta \mathrm{V_d} \Delta I_{\mathrm{s}} \approx \mathrm{V_{MPP}} \Delta I_{\mathrm{s}} = \mathrm{V_{MPP}} K \Delta \mathrm{s} \tag{21}$$

where ΔI_{s} is the array current variation (at a constant duty-cycle d(k)) due to the irradiance variation Δs and K is a material constant [1]. In order to avoid the failure of the P&O algorithm in dynamic conditions, on the basis of (15), (19), (20) and (21), the following inequality must be fulfilled

$$\left| -\left(\mathrm{H V_{MPP}} + \frac{1}{R_{\mathrm{MPP}}} \right) \right| (G_{\mathrm{o}} \cdot \Delta \mathrm{d})^2 > \mathrm{V_{MPP}} K |\Delta \mathrm{s}| \tag{22}$$

from which we get

$$\begin{aligned} \Delta \mathrm{d} &> \frac{1}{G_{\mathrm{o}}} \sqrt{\frac{\mathrm{V_{MPP}} k |\Delta S|}{\left(\mathrm{H V_{MPP}} + \frac{1}{R_{\mathrm{MPP}}} \right)}} \\ &= \frac{1}{G_{\mathrm{o}}} \sqrt{\frac{\mathrm{V_{MPP}} K |\dot{\mathrm{s}}| T_a}{\left(\mathrm{H V_{MPP}} + \frac{1}{R_{\mathrm{MPP}}} \right)}} \\ &= \Delta \mathrm{dmin} \end{aligned} \tag{23}$$

where $\dot{S}$ is the average rate of change of the irradiance level inside the time interval of length T_a (sampling period) between the k-th and the $(k+1)$-th sampling. The proper value to assign to T_a can be found on the basis of the considerations drawn in Section II; if inequality (23) is fulfilled, then, in the limit of validity of the approximations made, the P&O algorithm is able to track without errors irradiances characterized by average rates of change (within T_a) not higher than $\dot{S}$. The parameters H, $\mathrm{V_{MPP}}$ and R_{MPP} in (23) depend on the irradiance level: so that, when using (23), the combination of parameters (H, $\mathrm{V_{MPP}}$, R_{MPP}) leading to the highest value of the right-hand side must be used. In the sequel we will assume the following values for the parameters of system of Fig. 1: $\mathrm{H} = 2.2 \cdot 10^{-4}$ A/V^2 (at $S = 350$ W/m^2), $\mathrm{H} = 5.9 \cdot 10^{-4}$ A/V^2 (at $S = 1000$ W/m^2), $k = 6.895 \cdot 10^{-3}$ A $\cdot$ m^2/W, $\mathrm{V_{MPP}} = 290$ V (at $S = 1000$ W/m^2), $\mathrm{V_{MPP}} = 283$ (at $S = 350$ W/m^2). By assuming a constant rate of change $\dot{S} = 50\ \mathrm{W/(m^2 s)}$, the minimum value of Δd allowing the tracking of the irradiation without errors is equal to $\Delta\mathrm{dmin} = 0.008$. In Fig. 10(a) the behavior of the P&O driven duty-cycle in correspondence of the variation of the irradiance level from 350 W/m^2 to 1000 W/m^2 is shown, with a constant rate of change equal to $50\ \mathrm{W/(m^2 s)}$, $\Delta \mathrm{d} = 0.01 > \Delta\mathrm{dmin}$ and $T_a = 0.01$ s. As discussed in Section II, the value adopted for T_a allows the P&O algorithm working efficiently at steady-state. It is evident that, during the transient, the duty-cycle swings among more than three values [Fig. 10(b)]; in Section II it has been also shown that, at steady state, when a suitable value of T_a is chosen, the duty cycle oscillates assuming only three different values. Also in transient conditions, if the value of the amplitude of the duty-cycle perturbation is sufficiently high, then the duty-cycle oscillates assuming only three different values. The swing of the duty-cycle among four points in Fig. 10 is due to the fact that inequality (23) is approximate. Among the other approximations used to get (23), the main one is based on the assumption that the starting operating point is the MPP. Indeed, as the values assumed by the duty-cycle are quantized, the best operating point location only neighbors the MPP, as shown in Fig. 11. The degree of approximation involved in (23) deteriorates when the best operating point is located far from the MPP. Of course, by adopting a value of Δd much higher than the one provided by (23), we would succeed in getting a behavior characterized by the swinging of the duty-cycle among only three values but, at the same time, wider ocillations of the operating point around the MPP would appear with the consequent decrease of the efficiency. In conclusion, the behavior of

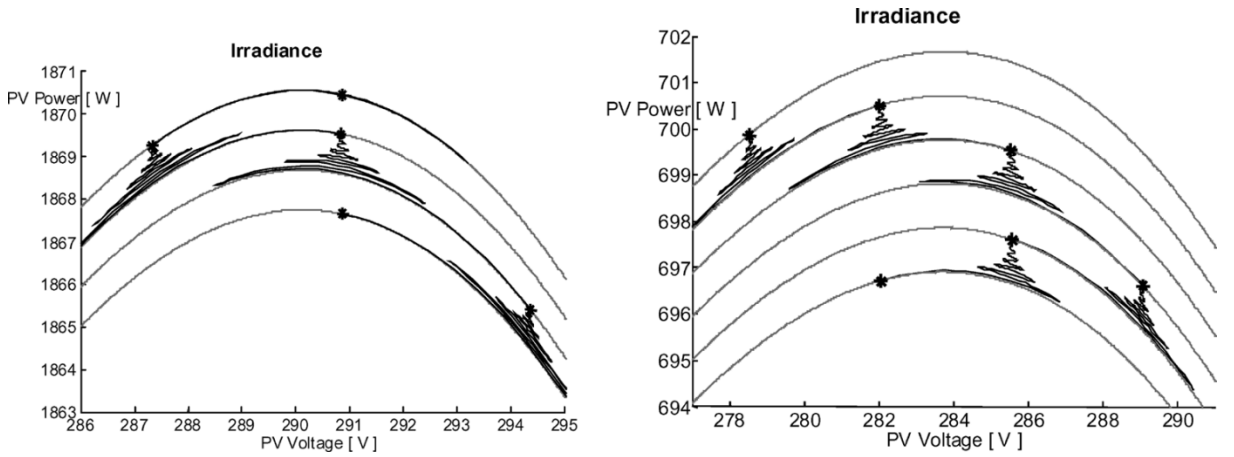

(a) (b)

Fig. 11. Operating point of PV battery charger with $T_a = 0.01$ s; $\Delta \mathrm{d} = 0.01$; $\dot{S} = 50$ W/(m^{2}s): (a) three points behavior and (b) four points behavior.

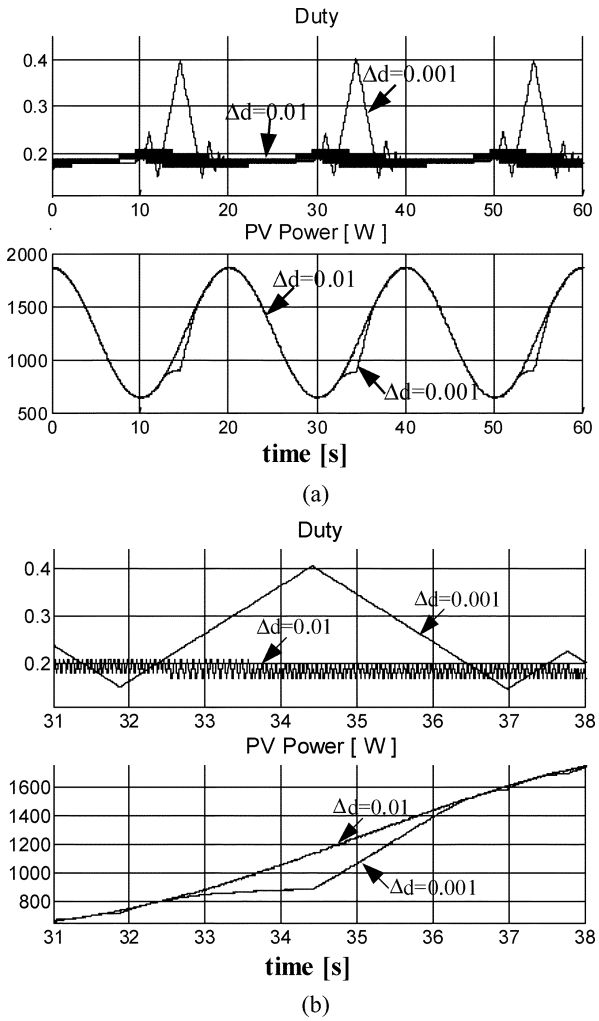

(a) (b)

Fig. 12. Time domain simulations: (a) $T_a = 0.01$ s; $\dot{S}_{\max} = 50$ W/(m^{2}s) and (b) zoom of (a).

the system shown in Fig. 10 is very efficient since no more than one extra step affects the swing across the MPP, compared with the best three-step case.

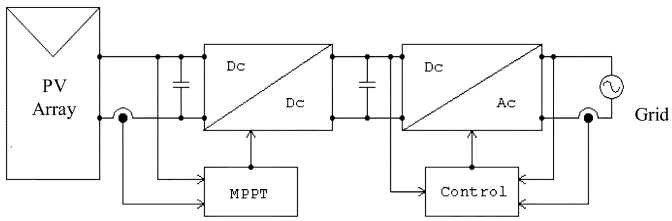

Fig. 13. Experimentally tested grid connected PV system.

In the case of four points behavior, the maximum voltage discrepancy between the operating point and the MPP is equal to $2\Delta \mathrm{V_d}$: so that, from (19) and (20), the corresponding maximum ΔP_{d} is

$$\begin{aligned}\Delta P_{\max} \cong & -\left(H \cdot V_{MPP} + \frac{1}{R_{MPP}}\right) \cdot (2 \cdot \Delta V_d)^2 \\ = & -\left(H \cdot V_{MPP} + \frac{1}{R_{MPP}}\right) \\ & \cdot (2 \cdot G_o \cdot \Delta d)^2. \end{aligned} \tag{24}$$

If the theoretical MPPT efficiency is defined as

$$\eta_{MPPT\%} = \left(1 - \frac{\Delta P_{\max}}{P_{MPP}}\right) \cdot 100 \tag{25}$$

then, in the case under study, with $\Delta \mathrm{d} = 0.01$ and $\dot{S} = 50$ W/(m^{2}s), it is $\eta_{MPPT\%} = 99.5\%$. Fig. 12 shows the behaviors of the P&O driven duty-cycle in correspondence of a sinusoidal time varying irradiance, characterized by a maximum rate of change equal to 50 W/(m^{2}s), in the two cases $\Delta \mathrm{d} = 0.01 > \Delta \mathrm{d_{min}}$ and $\Delta \mathrm{d} = 0.001 < \Delta \mathrm{d_{min}}$. Fig. 12 shows that, when (23) is not fulfilled ($\Delta \mathrm{d} = 0.001 < \Delta \mathrm{d_{min}}$), then the P&O algorithm fails to track the irradiance and a not negligible amount of available energy is wasted.

IV. Experimental Results

Fig. 13 shows a grid connected PV system adopted for experimental measurements.

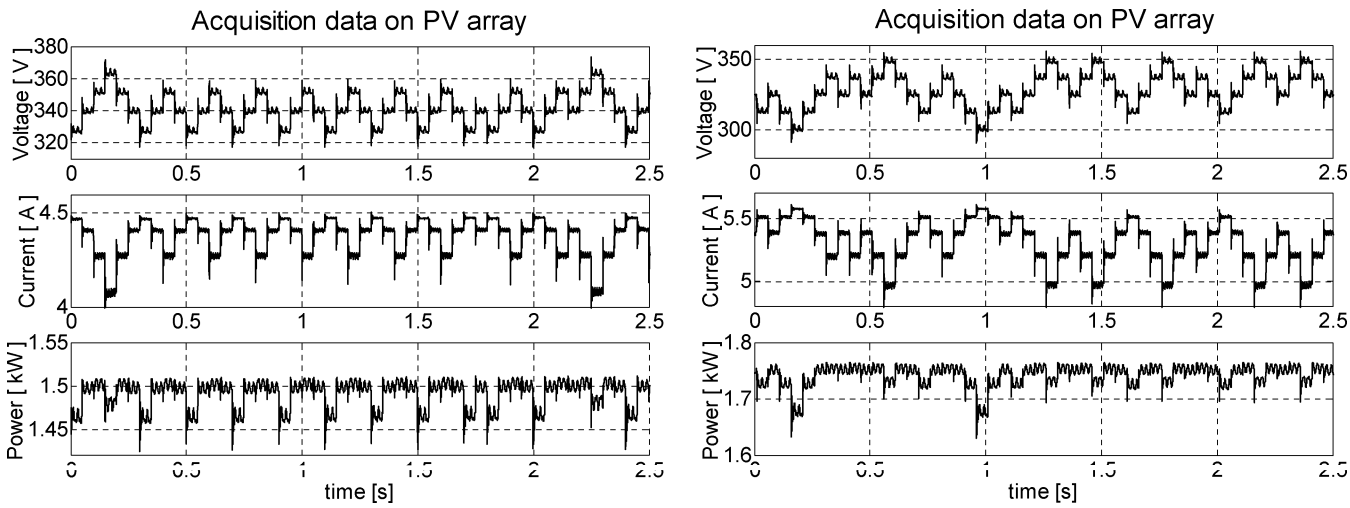

(a) (b)

Fig. 14. Experimental measurements: (a) clear day and (b) cloudy day.

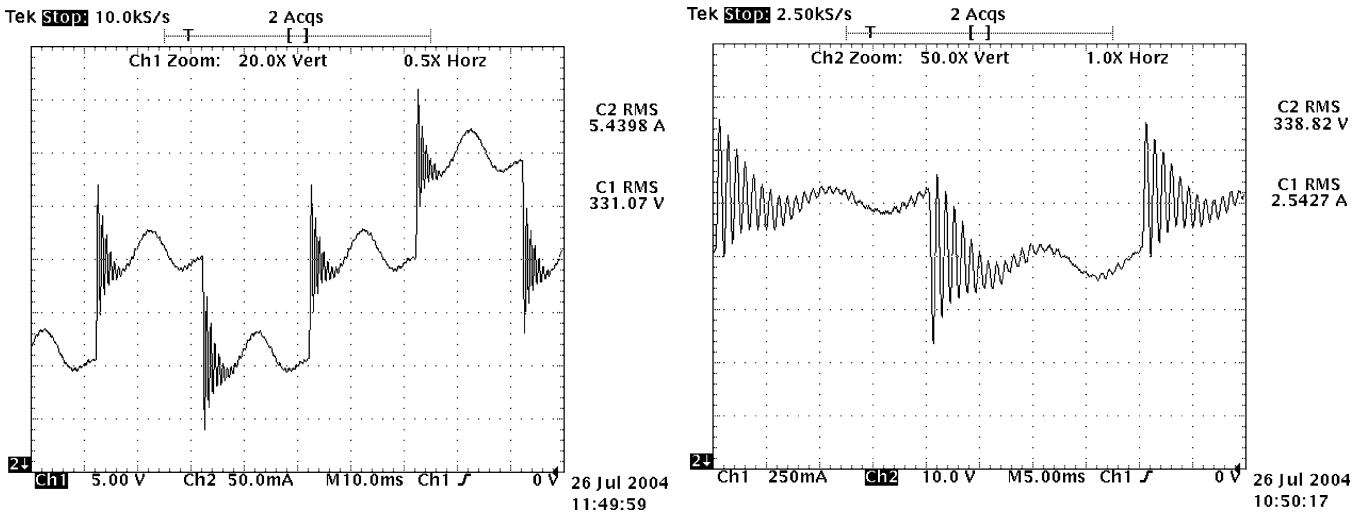

Fig. 15. Experimental PV voltage acquisition.

The boost MPPT converter supplies a 1.5 kW inverter for 220 V/50 Hz grid connection. In this case, the dc/ac section introduces a 100 Hz disturbance on the photovoltaic array voltage. This represents a worse operating condition for the mppt boost with respect to the case of the battery charger and allows to test the robustness of the proposed optimization method. The experimental time domain waveforms of $\mathrm{v}_{PV}i_{\mathrm{PV}}$ and P_{PV} are shown in Fig. 14.

Data acquisitions during a clear day [Fig. 14(a)] show a three points swinging MPPT control, with some occasional corrections by means of a further level. Nevertheless, even with a voltage swing of about 40 V, the power swing under its maximum value does not exceed 40 W. Fig. 14(b) shows the operating point swings during a cloudy day. Fig. 15 shows a more detailed plot of PV voltage. The high frequency oscillations are due to the effect of the duty cycle step wise perturbation, weighted by $G_{v_p^d}$, [first right-hand side term of (9)]. Instead, the slower oscillations, at 100 Hz, represent the effect of the second right-hand side term of (9). In this case, the best MPPT parameters are $\Delta \mathrm{d} = 0.05$ and $T_a = 20$ ms. By using (24) with $\Delta \mathrm{V_d} \cong 10$ V, consistent with the values shown in Fig. 15, a $\Delta P_{\max}$ equal to about 90 W is obtained. This prediction, based on a four point swinging MPPT control, is confirmed by both plots of PV power of Fig. 14(a) and (b).

V. Conclusion

In this paper a theoretical analysis allowing the optimal choice of the two main parameters characterizing the P&O algorithm has been carried out. The idea underlying the proposed optimization approach lies in the customization of the P&O MPPT parameters to the dynamic behavior of the whole system composed by the specific converter and PV array adopted. The results obtained by means of such approach clearly show that in the design of efficient MPPT regulators the easiness and flexibility of P&O MPPT control technique can be exploited by optimizing it according to the specific system's dynamic characteristics. As an example a boost converter has been examined. The results obtained and the considerations drawn can be extended to any other converter topology as well.

ACKNOWLEDGMENT

The authors wish to thank Dr. F. De Rosa for his precious cooperation.

REFERENCES

[1] S. Liu and R. A. Dougal, "Dynamic multiphysics model for solar array," *IEEE Trans. Energy Conv.*, vol. 17, no. 2, pp. 285–294, Jun. 2002.

[2] K. H. Hussein, I. Muta, T. Hshino, and M. Osakada, "Maximum photovoltaic power tracking: an algorithm for rapidly changing atmospheric conditions," *Proc. Inst. Elect. Eng.*, vol. 142, no. 1, pp. 59–64, Jan. 1995.

[3] M. Veerachary, T. Senjyu, and K. Uezato, "Voltage-based maximum power point tracking control of PV system," *IEEE Trans. Aerosp. Electron. Syst.*, vol. 38, no. 1, pp. 262–270, Jan. 2002.

[4] K. K. Tse, M. T. Ho, H. S.-H. Chung, and S. Y. Hui, "A novel maximum power point tracker for PV panels using switching frequency modulation," *IEEE Trans. Power Electron.*, vol. 17, no. 6, pp. 980–989, Nov. 2002.

[5] P. Midya, P. Krein, R. Turnbull, R. Reppa, and J. Kimball, "Dynamic maximum power point tracker for photovoltaic applications," in *Proc. 27th Annu. IEEE Power Electronics Specialists Conf.*, vol. 2, Jun. 1996, pp. 1710–1716.

[6] E. Koutroulis, K. Kalaitzakis, and N. C. Voulgaris, "Development of a microcontroller-based, photovoltaic maximum power point tracking control system," *IEEE Trans. Power Electron.*, vol. 16, no. 1, pp. 46–54, Jan. 2001.

[7] T. Noguchi, S. Togashi, and R. Nakamoto, "Short-current pulse-based maximum-power-point tracking method for multiple photovoltaic-and-converter module system," *IEEE Trans. Ind. Electron.*, vol. 49, no. 1, pp. 217–223, Feb. 2002.

[8] K. Irisawa, T. Saito, I. Takano, and Y. Sawada, "Maximum power point tracking control of photovoltaic generation system under nonuniform insolation by means of monitoring cells," in *Proc. 28th IEEE Photovoltaic Specialists Conf.*, Sep. 2000, pp. 1707–1710.

[9] C. Hua, J. Lin, and C. Shen, "Implementation of a DSP-controlled photovoltaic system with peak power tracking," *IEEE Trans. Ind. Electron.*, vol. 45, no. 1, pp. 99–107, Feb. 1998.

[10] T. Wu, C. Chang, and Y. Chen, "A fuzzy-logic-controlled single-stage converter for PV-powered lighting system applications," *IEEE Trans. Ind. Electron.*, vol. 47, no. 2, pp. 287–296, Apr. 2000.

[11] I. Batarseh, T. Kasparis, K. Rustom, W. Qiu, N. Pongratananukul, and W. Wu, "DSP-based multiple peak power tracking for expandable power system," in *Proc. 18th Annu. IEEE Applied Power Electronics Conf. Expo*, vol. 1, Feb. 2003, pp. 525–530.

[12] D. P. Hohm and M. E. Ropp, "Comparative study of maximum power point tracking algorithms," in *Proc. 28th IEEE Photovoltaic Specialists Conf.*, Sep. 2000, pp. 1699–1702.

[13] C. A. Desoer and E. S. Kuh, *Basic Circuit Theory*. New York: McGraw-Hill, 1969.

[14] R. W. Erickson and D. Maksimović, *Fundamental of Power Electronics*. Norwell, MA: Kluwer, 2001.

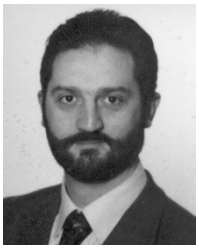

Nicola Femia (M'94) was born in Salerno, Italy, in 1963. He received the Ph.D. degree (with honors) in engineering of industrial technologies from the University of Salerno, Italy, in 1988.

From 1990 to 1998, he was an Assistant Professor, from 1998 to 2001, he was an Associate Professor, and since 2001 has been a Full Professor of electrotechnics at the Faculty of Engineering, University of Salerno. He is coauthor of about 80 scientific papers published in the proceedings of international symposia and in international journals. His main scientific interests are in the fields of circuit theory and applications and power electronics.

Dr. Femia was an Associate Editor of the IEEE TRANSACTIONS ON POWER ELECTRONICS from 1995 to 2003.

Giovanni Petrone was born in Salerno, Italy, in 1975. He received the "Laurea" degree in electronic engineering from the University of Salerno, Italy, in 2001 and the Ph.D. degree in electrical engineering from the University of Napoli "Federico II," Italy, in 2004.

Since March 2004, he has collaborated with the Electrical Engineering Department, University of Salerno. His main research interests are in the analysis and design of switching converters for telecommunication applications, renewable energy sources in distributed power systems, and tolerance analysis of electronic circuits.

Giovanni Spagnuolo (M'98) was born in Salerno, Italy, in 1967. He received the "Laurea" degree in electronic engineering from the University of Salerno, Italy, in 1993 and the Ph.D. in electrical engineering from the University of Napoli, "Federico II," Italy, in 1997.

From November 1993 to October 1994, he was a Researcher on the design, building, and tuning of a high voltage test-bed of a cryogenic superconducting cable. In 1993, he joined the Dipartimento di Ingegneria dell'Informazione ed Ingegneria Elettrica, University of Salerno, where he was a Post-Doctoral Fellow (1998–1999), an Assistant Professor of Electrotechnics (1999–2003) and, since January 2004, an Associate Professor. His main research interests are in numerical methods for the analysis of electromagnetic fields, in the analysis and simulation of switching converters and in tolerance analysis and design of electronic circuits.

Massimo Vitelli was born in Caserta, Italy, in 1967. He received the "Laurea" degree (with honors) in electrical engineering from the University of Naples, "Federico II," Italy, in 1992.

In 1994, he joined the Department of Information Engineering, Second University of Naples, as a Researcher. In 2001, he was appointed Associate Professor in the Faculty of Engineering, Second University of Naples, where he teaches Electrotechnics. His main research interests concern the electromagnetic characterization of new insulating and semi-conducting materials for electrical applications, electromagnetic compatibility and the analysis and simulation of power electronic circuits.

Dr. Vitelli is an Associate Editor of the IEEE TRANSACTIONS ON POWER ELECTRONICS.